ARTICLE

Significant Carrier Concentration Changes in Native Electrodeposited ZnO

Shawn Chatman, Lisa Emberley, and Kristin M. Poduska*

Department of Physics and Physical Oceanography, Memorial University of Newfoundland, St. John's, Newfoundland A1B 3X7, Canada

ABSTRACT We show that unintentional hydrogen doping of ZnO during the electrodeposition process can impact the material's carrier concentration as significantly as others have reported for intentional extrinsic doping. Mott–Schottky analyses on the natively n-type electrodeposits show a decrease in the carrier concentrations from 10^{21} to 10^{18} cm^{-3} with increasing overpotential. A strong link exists between larger optical band gaps (determined from diffuse reflectance spectroscopy) and higher carrier concentrations, which suggests that hydrogen-based doping underlies the n-type conductivity (Moss–Burstein effect). We propose that kinetic defects introduced during growth at larger overpotentials compete with hydrogen doping, thereby leading to lower net carrier concentrations. This has important implications for using the deposition potential to tune other electrodeposit properties such as the growth rate and morphology.

KEYWORDS: ZnO • carrier concentration • hydrogen doping • band gap • electrodeposition • X-ray diffraction

INTRODUCTION

Transparent semiconducting materials are the cornerstone of many optoelectronic devices, including those used in the photovoltaic industry (1). In these applications, reliable control of the carrier concentration is essential to optimize both optical transparency and electrical conductivity (2). Electrochemical deposition of transparent semiconductors is gaining acceptance as a viable means of producing films of transparent semiconducting metal oxides such as ZnO and TiO_2 (3). However, there is still much to be understood about how to control carrier concentrations in these electrodeposited materials. Here, we show that the carrier concentration of native electrodeposited ZnO can be modified over several orders of magnitude simply by changing the potential applied during deposition. Our results show an approach to n doping that yields a similar range of carrier concentrations without introducing intentional dopants. The implications are that using potential to control other features of the electrodeposit, such as growth rate or morphology, may simultaneously affect the deposit's electronic properties.

ZnO is a well-studied wide-band-gap material that is n-type in its native form (2, 4). Considerable scientific effort has been devoted to understanding how and why hydrogen is the cause of this n-type doping (5, 6). Hydrogen is expected to be an amphoteric dopant in most materials by compensating for existing defects. In ZnO, however, electronically active interstitial H^+ serves as a donor (7) and increases the band-gap energy when doping levels are high enough to lead to degenerate semiconducting behavior. This Moss–Burstein effect (8) of larger band gaps with higher doping levels is a trend that opposes the usual response of decreasing band gap with an increase in extrinsic dopants (as has been observed in boron-doped ZnO (9) and, more recently, with Cl^- in ZnO electrodeposits (10)).

This work, based on Mott–Schottky (M–S) analyses, shows that significant changes in the carrier concentration can be induced in native ZnO electrodeposits without introducing intentional dopants. Because the hydrogen evolution reaction (HER) proceeds concurrently with ZnO electrosynthesis, there is an obvious presence of hydrogen. However, there are no existing studies that address its effect on the carrier concentration.

EXPERIMENTAL METHODS

ZnO Electrosynthesis. ZnO thin films were deposited from aqueous electrolytes using a precipitation/reduction reaction process reported by Izaki et al. (9) and modified by our research group (4, 5).

$$NO_3^- + H_2O + 2e^- \rightarrow NO_2^- + 2OH^- \quad (1)$$

$$Zn^{2+} + 2OH^- \rightarrow Zn(OH)_2 \rightarrow ZnO + H_2O \quad (2)$$

During this reaction, nitrate ions are reduced to nitrite ions in the presence of Zn^{2+} adsorbed on the surface of the working electrode (14). Consequently, excess hydroxide ions are produced, increasing the local pH. This pH increase facilitates the formation of $Zn(OH)_2$ on the working electrode, which spontaneously decomposes to ZnO at temperatures above 50 °C (14, 15).

ZnO samples were synthesized from 0.01 M $Zn(NO_3)_2$ (ACS reagent grade, SCP Science in 18.2 MΩ·cm water, Barnstead Nanopure). The electrolyte pH was controlled by the addition of HCl (pH = 4.0–5.5) or NaOH (pH = 6.0–7.5). Deposition potentials, ranging from −1.3 to −0.85 V, are all reported relative to a Ag/AgCl reference. Substrates consisted of mechanically polished stainless steel (316 stainless steel or A286 steel alloy) that was ultrasonically cleaned prior to use.

* E-mail: kris@mun.ca. Phone: (709)-737-8890. Fax: (709)-737-8739.
Received for review July 23, 2009 and accepted September 15, 2009

DOI: 10.1021/am900491v

Published on Web 09/30/2009

Structural, Morphological, and Optical Characterization. X-ray diffraction (XRD) data were collected using a Debye−Scherrer powder diffractometer (Rigaku D/MAX 2200 PC) in $\theta-\theta$ geometry using Cu Kα radiation. Diffraction data were collected over $2\theta = 20-80°$, with a 0.03° 2θ step size at 6°/min.

Scanning electron microscopy (SEM) was performed with a Hitachi S570 scanning electron microscope and a digital imaging collector. Deposit thicknesses were extracted from contact-mode atomic force microscopy data taken with an Asylum Research MFP-3D system using a silicon tip (μMasch CSC37/Cr−Au with a spring constant of 0.1−0.4 N/m).

Diffuse-reflectance spectroscopy data were collected using a Ocean Optics USB2000 spectrometer. The diffuse-reflectance setup uses a UV/visible light source surrounded by collectors incident upon the sample at 45°. ZnO band gaps were calculated from reflectance data by differentiating the reflectance intensity at the optical edge with respect to energy and by taking the peak position of the first derivative because other studies have shown that band-gap values obtained with this method are closer to the true values obtained from transmission measurements (7).

Carrier Concentration Measurements. M−S analysis, based on the concept of impedance spectroscopy, utilizes the relationship between the capacitance and applied potential to extract information about a material's carrier concentration. This technique has been applied to nanostructured (9, 10) as well as Cl-doped (10) ZnO.

M−S analysis assesses carrier concentrations near a rectifying (nonohmic, Schottky) junction at the surface of the semiconductor; in our experiments, this was achieved at the semiconductor/electrolyte interface. For Schottky junctions, theory dictates that the reciprocal of the junction capacitance squared will vary linearly with the applied reverse bias, as shown here (and derived in the Supporting Information):

$$\left(\frac{1}{C}\right)^2 = \frac{2V_{bi} + V_R}{e\varepsilon_s a^2 N_d} \tag{3}$$

Here C is the junction capacitance, V_R is the applied reverse bias voltage, V_{bi} is the built-in potential, a is the surface area of the junction, e is the elemental charge, N_d is the carrier concentration, and ε_s is the semiconductor's dielectric constant, which we take to be 8.0 for bulk ZnO (9). In reality, extra terms must be added to account for additional capacitive effects due to classic dielectric capacitance, C_d, as well as the "double-layer" capacitance, C_{dl} (due to an accumulation of ions at the surface of the working electrode), and capacitance due to fractional coverage or a conducting substrate (f) and increased surface area fraction due to roughness (g, where, for example, $g = 1.5$ would indicate a 50% increase in the surface area due to roughness) (19):

$$\left(\frac{1}{C}\right)^2 = \frac{2V_{bi} + V_R}{e\varepsilon_s a^2 N_d} + (1-f)\frac{1}{{C_{dl}}^2} + f\left(\frac{1}{C_d} + \frac{1}{gC_{dl}}\right)^2 \tag{4}$$

Because these additional capacitance terms change the intercept, but not the slope, of eq 3, it is not necessary to quantify all auxiliary capacitances in order to determine the carrier concentration.

Accounting for the true surface area, a, of ZnO in contact with the electrolyte requires prudent approximations. We assume that the planar surface area (as used in other investigations (1) of ZnO electrodeposits) is an underestimation of the true surface area, suggesting that the carrier concentrations determined from our M−S data are upper limits. Therefore, we focus on trends and order of magnitude variations in the carrier concentrations rather than on specific values. A more comprehensive discussion of roughness effects on the carrier concentration calculations is included in the Supporting Information.

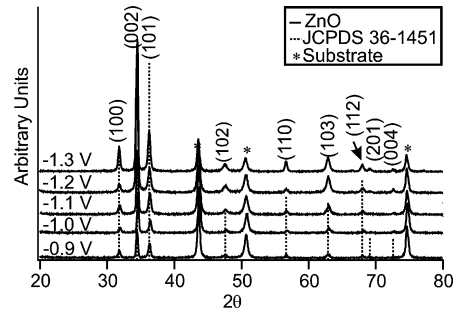

FIGURE 1. Representative indexed XRD patterns from electrodeposited ZnO prepared at pH 6.5 with deposition potentials ranging from −1.3 to −0.9 V vs Ag/AgCl. Refined lattice constants for electrodeposits deposited over the complete range of deposition conditions compared well with the accepted values (a = 3.250 Å and c = 5.207 Å, JCPDS no. 36-1451). Plots are offset along the intensity axis for clarity.

M−S analyses were performed in the electrolyte by superimposing an alternating current at 10−15 kHz with a peak-to-peak voltage of 20 mV over a stepped potential ranging from −1 to +1.3 V vs Ag/AgCl and measuring the resulting impedance. Capacitance values were extracted from impedance data using the relationship

$$C = \frac{1}{j\omega Z} \tag{5}$$

M−S experiments were controlled by, and data were collected with, the *PowerSUITE* [EG&G Princeton Applied Research (PAR)] impedance spectroscopy software package interfaced with a PAR 273A potentiostat and Signal Recovery 5210 lock-in amplifier. Several supporting electrolytes were tested for their suitability for these M−S experiments. The native electrolyte [pH-adjusted 0.01 M $Zn(NO_3)_2$], as used by Windisch et al. (9), contributes capacitance fluctuations due to both the nitrate reduction reaction and Zn^{2+} adsorption (20). A better alternative was a modified phosphate buffer, similar to the one reported recently (10), consisting of 0.063 M K_2PO_4 + 0.036 M NaOH, which has a pH of 7. All M−S data shown here were collected using this buffered phosphate electrolyte.

RESULTS

The electrodeposition process yields ZnO thin films whose lattice constants were refined to 3.246 ± 0.001 Å and c = 5.205 ± 0.002 Å, which is in excellent agreement with JCPDS no. 36-1451 for ZnO (3.250 and 5.207 Å) (21). The refined lattice constants were consistent for samples deposited over a range of pH values (5.5−7.5) and deposition potentials (−1.3 to −0.85 V), consistent with previous results from our group over a more acidic pH range (4−5.5) (5). Qualitative comparisons of relative peak heights (Figure 1) also confirmed that, while our samples are polycrystalline, there is a preferred (002) orientation in the deposit, which is typical for electrodeposited ZnO (4, 15, 22). This (002) texture is moderately accentuated for samples deposited at −1.1 V (pH 6.5), coinciding with a morphological change

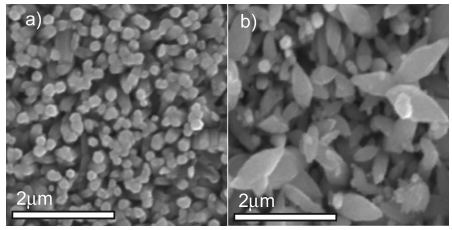

FIGURE 2. Representative SEM micrographs of ZnO samples deposited at (a) −0.9 V in a pH 6.5 electrolyte and (b) −1.3 V in a pH 5 electrolyte. The hexagonal columns in part a are typical of deposits from neutral pH electrolytes and more positive deposition potentials, while the ricelike morphologies are observed at more negative potentials and more acidic pH values.

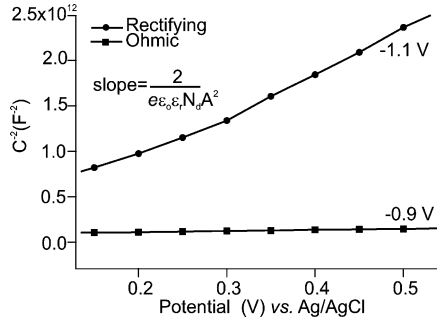

FIGURE 3. Representative C^{2-} vs potential plots obtained from solution M−S analyses performed on electrodeposited ZnO samples in a pH 7 phosphate buffer. The uncertainties associated with individual data points are smaller than the uncertainty calculated from the subsequent linear regression analysis.

from hexagonal crystallites to ricelike structures, as shown in Figure 2 and reported previously (4).

Despite the fact that XRD shows no obvious structural differences among samples prepared over this potential (−0.9 to −1.3 V) and pH range (pH 4−7), we find drastically different carrier concentrations based on M−S analyses. Representative M−S plots for samples deposited at low (−1.1 V) and high (−0.9 V) applied potentials (from a pH 6.5 electrolyte) are shown in Figure 3, corresponding to carrier concentrations of 8.7×10^{20} cm^{-3} and 2.3×10^{19} cm^{-3}, respectively. Over a range of applied deposition potentials (all in a pH 6.5 electrolyte), there is a clear trend of decreasing carrier concentration with more negative deposition potentials, as shown in Figure 4a. Comparing data from electrodeposits prepared at different pH values, Figure 4b shows the carrier concentration versus the standard potential of the HER. Because the potential at which hydrogen evolves in solution is dependent upon the pH, this effectively couples the potential and pH, allowing a more direct comparison of the carrier concentration change with deposition conditions. Both parts a and b of Figure 4 show that the carrier concentration decreases with increasing overpotential (with respect to HER). This relationship was established based on the measurements of dozens of samples. Carrier concentrations were calculated from the linear section of the M−S graphs, to eliminate the possibility of including data collected under complete depletion. We confirmed that deposit thicknesses (0.5−3.0 μm) were all substantially larger than depletion layer thicknesses, even

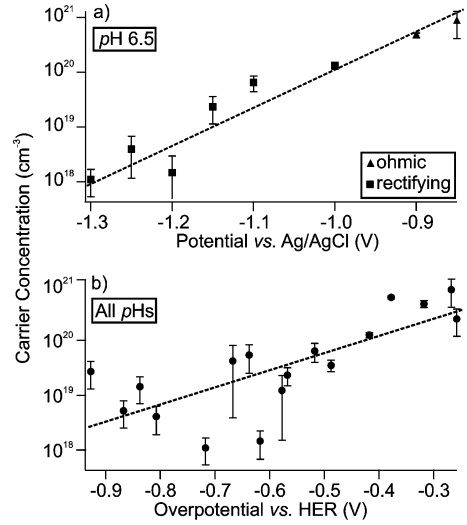

FIGURE 4. Carrier concentrations determined by solution M−S analyses indicating a monotonic increase in the carrier concentration with more positive deposition potentials. This figure shows plots of log carrier concentration vs overpotential (a) at pH 6.5 and (b) for all pH conditions.

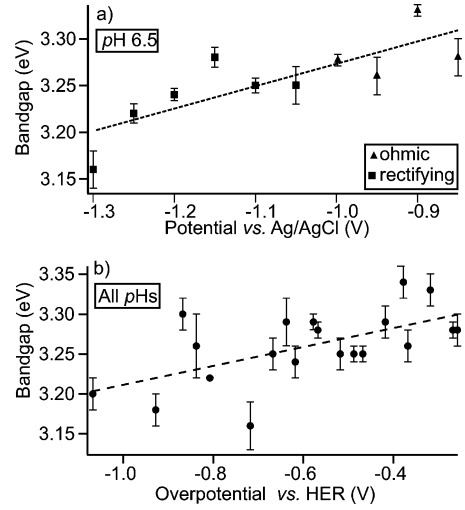

FIGURE 5. UV/visible diffuse-reflectance analysis was used to collect sample band-gap values. Our data indicate a monotonic increase in the band gap with more positive deposition potentials (a) for samples deposited at pH 6.5 (plotted vs Ag/AgCl reference) and (b) for all samples (the water electrolysis standard potential).

for the lowest carrier concentrations (80 nm at 10^{17} cm^{-3} to 8 Å at 10^{21} cm^{-3}).

Because carrier concentration changes can influence optical as well as electronic properties, we also compared trends in optical absorption edges, obtained from diffuse-reflectance spectra, with electrodeposition conditions. Samples deposited at more positive potentials exhibited larger band gaps than samples deposited at more negative deposition potentials, as can be seen in parts a (samples synthesized at pH 6.5) and b (all samples) of Figure 5. Optical band gaps ranged between 3.1 and 3.4 eV, which is in agreement with values reported for the band gap of ZnO (2, 7, 9, 10). We do not observe changes in the band gap with changes in the sample thickness between 0.5 and 3.0 μm. Although others (7) have reported thickness-dependent band gaps, their electrodeposits also show thickness-dependent changes in

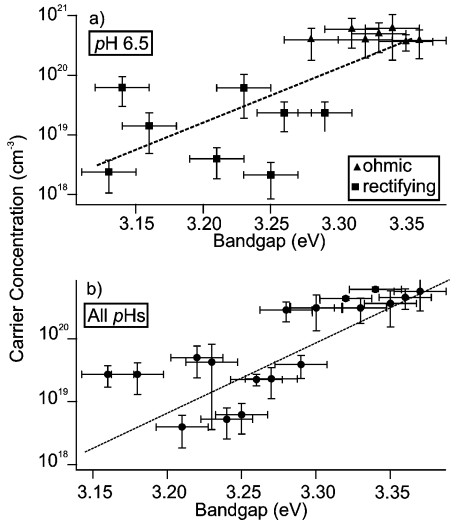

FIGURE 6. Plot of log carrier concentration vs band gap for deposition at pH 6.5 (a) and all pH conditions (b). The line serves as a guide to the eye.

the texture, morphology, and unit cell size that we do not observe in our electrodeposits. Additional discussions of the role of the deposit thickness on optical band-gap values are included in the Supporting Information.

We note that built-in potentials could not be determined from our M−S plots because of a sample-dependent constant capacitance term. This may be due to variations in the electrodeposit coverage (parameter *f* in eq 4) because earlier studies (5) have shown that small pinholes can occur in our electrodeposits. Fabregat-Santiago et al. have also shown that sample-dependent capacitance can occur when there are sample/electrolyte interactions (19).

DISCUSSION

Over the entire range of deposition potentials (−1.3 to −0.85 V) and pH values (4.0−7.5) studied, ZnO carrier concentrations ranged between 10^{17} and 10^{20} cm^{-3}. This range is in agreement with reported carrier concentrations for ZnO (9, 10), including ZnO electrodeposited from nitrate-based electrolytes (9, 10).

Our results indicate a higher n-type carrier concentration in ZnO that is electrodeposited at more positive deposition potentials. While some electrolytes, such as those containing Cl^- or borane (9, 10), offer a clear opportunity for extrinsic doping, the same cannot be said for our nitrate-based electrolyte. Instead, it is much more likely that hydrogen is incorporated as an n-type dopant. We support this claim by correlating the trends in the carrier concentration and optical band gap with respect to the deposition potential.

Figure 6 shows that the band gaps of our ZnO electrodeposits increase with increasing carrier concentration. In the context of traditional donor/acceptor band theory, a decreased band gap would indicate an increased carrier concentration, as has been observed recently with Cl-doped ZnO electrodeposits (10). However, hydrogen doping in ZnO has been observed to go against this trend (5, 6). Hydrogen-donated electrons can fill empty states in the conduction band of ZnO when doping levels are high enough to create a degenerate semiconductor, thereby leading to increased band gaps with higher doping levels (the Moss−Burstein effect) (4, 8). Our data are consistent with this Moss−Burstein doping, whether for a single pH (Figure 6a for samples deposited at pH 6.5 from a Cl^--free electrolyte) or over our whole range of deposition conditions (Figure 6b).

If we use the band gap versus potential trend to attribute the increasing carrier concentration to higher H^+ doping levels, we arrive at an interesting, and rather counterintuitive, finding. Intuitively, one could reasonably expect that an increase in hydrogen generation would translate into more incorporated hydrogen and, consequently, a higher carrier concentration. However, we observe higher carrier concentrations at more positive deposition potentials, where there should be a lower rate of hydrogen generation (23). Thus, our findings suggest that the relationship between the carrier concentration and the presence of hydrogen during the electrosynthesis process is more complicated.

One likely complicating factor is the presence of multiple types of defects. While recent studies indicate that hydrogen donors are an energetically favorable dopant, and thus the most dominant factor in the n-type doping in ZnO, there is experimental evidence that supports the prevalence of oxygen and zinc vacancy, interstitial, and antisite defect contributions (24). Of these intrinsic point defects, it is known that zinc vacancies, oxygen interstitials, and oxygen antisites act as deep acceptors within ZnO while oxygen vacancies, zinc interstitials, and zinc antisites act as donors. In fact, it has been found that in ZnO the formation of acceptor defects is energetically preferable to the formation of native donor defects (25, 26). Zinc vacancy acceptors require the lowest formation energies of the three acceptor defects, and they are also stable to temperatures of 300 °C, which is far above our electrodeposition temperatures. Consequently, zinc vacancies would be the most likely kind of acceptor defect, according to thermodynamic arguments, and these acceptors could compensate for, and thus diminish the overall effect of, increased hydrogen incorporation. Previous studies have confirmed that the presence of deep acceptors in ZnO crystals will be active toward hydrogen passivation in ZnO (7, 27).

If we adopt the working hypothesis that compensating defects could reduce the net n-type carrier concentration, it is reasonable to expect that these defects would be more prevalent at more negative deposition potentials. Reaction kinetics will be faster at greater overpotentials, and this increase in the synthesis rate would likely contribute to an increase in the defect densities. This is indeed consistent with the results shown in Figure 6.

Although hydrogen is now widely recognized as a prevalent dopant in ZnO, it is still an open question where and how hydrogen is incorporated. Theoretical studies (7) have suggested locations for interstitial hydrogen, and data from IR and Raman spectroscopic measurements (28) have shown evidence of hydrogen incorporation. Computational investigations of hydrogen diffusion in ZnO (29), however, indicate that hydrogen complexation is likely based on the

surprising thermal stability of incorporated hydrogen (up to 400 °C in some ZnO samples). In our samples, the resistance and carrier concentration values are consistent over the span of months. Others have observed optical and electronic effects of hydrogen diffusion over the span of days to weeks (4, 28). Because annealing can change not only the hydrogen content but also the surface structure, grain size, and oxygen content, it is not straightforward to ascribe annealing-related changes in the carrier concentration to changes in the hydrogen content alone. Thus, pinpointing likely locations and chemical environments for hydrogen in the lattice is an ongoing challenge for all who work with ZnO.

CONCLUSIONS

The large changes in the carrier concentrations of native (unintentionally doped) electrodeposited ZnO are comparable to the effect of intentional extrinsic dopants like Cl^- or borates. Because we observe that higher n-type carrier concentrations coincide with larger optical band gaps, we attribute the unintentional defects to the Moss–Burstein dopant hydrogen. Our data also indicate that both the net carrier concentration and band gap are lower in samples deposited at more negative deposition potentials, contrary to the increase in hydrogen generation at more negative deposition potentials. We attribute this trend to the higher deep acceptor defect densities of samples deposited at more negative deposition potentials and their faster reaction kinetics.

There are inherent difficulties in quantitative assessments of hydrogen incorporation in semiconductors, particularly in assessing the hydrogen coordination environment, mobility, and complexation. For this reason, the study of donor and acceptor defects is receiving considerable attention from the scientific community (6, 25), both theoretically and experimentally. The results of the present study highlight the need for a better understanding of the interplay between native defects and external dopants.

Acknowledgment. We thank H. Gillespie (XRD) and L. Men (SEM) for use of instrument facilities at Memorial University of Newfoundland. We also acknowledge financial support from the Natural Science and Engineering Resource Council (Canada), Canada Foundation for Innovation New Opportunities Fund, and Memorial University of Newfoundland.

Supporting Information Available: Derivation of the M–S capacitance relations and its relation to the sample roughness, an explanation of the biased steel/ZnO/electrolyte junction characteristics, and a discussion of the effects of the deposit thickness. This material is available free of charge via the Internet at http://pubs.acs.org.

REFERENCES AND NOTES

(1) Surek, T. *J. Cryst. Growth* **2005**, *275*, 292–304.
(2) Özgür, Ü.; Alivov, Ya. I.; Liu, C.; Teke, A.; Reshchikov, M. A.; Dogan, S.; Avrutin, V.; Cho, S.-J.; Morkoç, H. *J. Appl. Phys.* **2005**, *98*, 041301/1-103.
(3) Lincot, D. *Thin Solid Films* **2005**, *487*, 40–48.
(4) Ellmer, K. *J. Phys. D: Appl. Phys.* **2001**, *34*, 3097–3108.
(5) Van de Walle, C. G.; Neugebauer, J. *Nature* **2003**, *423*, 626–628.
(6) Chambers, S. A. *Surf. Sci.* **2007**, *601*, 5313–5314.
(7) Van de Walle, C. G. *Phys. Rev. Lett.* **2000**, *85*, 1012–1015.
(8) Burstein, E. *Phys. Rev.* **1954**, *93*, 632–633.
(9) Ishizaki, H.; Imaizumi, M.; Matsuda, S.; Izaki, M.; Ito, T. *Thin Solid Films* **2002**, *411*, 65–68.
(10) Rousset, J.; Saucedo, E.; Lincot, D. *Chem. Mater.* **2009**, *21*, 534–540.
(11) Izaki, M.; Omi, T. *Appl. Phys. Lett.* **1996**, *68*, 2439–2440.
(12) Ren, T.; Baker, H. R.; Poduska, K. M. *Thin Solid Films* **2007**, *515*, 7976–7983.
(13) Chatman, S.; Poduska, K. M. *ACS Appl. Mater. Interfaces* **2009**, *1*, 552–558.
(14) Yoshida, T.; Komatsu, D.; Shimokawa, N.; Minoura, H. *Thin Solid Films* **2004**, *451–452*, 166–169.
(15) Limmer, S. J.; Kulp, E. A.; Switzer, J. A. *Langmuir* **2006**, *22*, 10535–10539.
(16) Marotti, R.; Guerra, D.; Bello, C.; Machado, G.; Dalchiele, E. *Sol. Energy Mater. Sol. Cells* **2004**, *82*, 85–103.
(17) Mora-Seró, I.; Fabregat-Santiago, F.; Denier, B.; Bisquert, J.; Tena-Zaera, R.; Elias, J.; Levy-Clement, C. *Appl. Phys. Lett.* **2006**, *89*, 203117/1-3.
(18) Windsich, C. F.; Exarhos, G. J. *J. Vac. Sci. Technol., A* **1999**, *18*, 1677–1680.
(19) Fabregat-Santiago, F.; Garcia-Belmonte, G.; Bisquert, J.; Bogdanoff, P.; Zaban, A. *J. Electrochem. Soc.* **2003**, *150*, E293–E298.
(20) Pajkossy, T. *Solid State Ionics* **2005**, *176*, 1997–2003.
(21) Joint Commission on Powder Diffraction Standards—International Centre for Diffraction Data, "Powder Diffraction File", 2003.
(22) Peulon, S.; Lincot, D. *J. Electrochem. Soc.* **1998**, *145*, 864–874.
(23) Bard, A. J.; Faulkner, L. R. *Electrochemical Methods: Fundamentals and Applications*; John Wiley: New York, 2001.
(24) Vlasenko, L. S.; Watkins, G. D. *Phys. Rev. B: Condens. Matter* **2005**, *72*, 035203.
(25) Janotti, A.; Van de Walle, C. G. *Phys. Rev. B: Condens. Matter* **2007**, *76*, 165202/1–22.
(26) Oba, F.; Nishitani, S. R.; Isotani, S.; Adachi, H.; Tanaka, I. *J. Appl. Phys.* **2001**, *90*, 824–828.
(27) Lavrov, E. V.; Weber, J.; Börrnert, F.; Van de Walle, C. G.; Helbig, R. *Phys. Rev. B: Condens. Matter* **2002**, *66*, 165205/1-7.
(28) Jokela, S. J.; McCluskey, M. D. *Physica B* **2007**, *401–402*, 395–398.
(29) Wardle, M. G.; Goss, J. P.; Briddon, P. R. *Phys. Rev. Lett.* **2006**, *96*, 205504/1-4.

AM900491V